Polarized Oxygen K_α and Copper L_α X-Ray Emission Spectroscopy of $YBa_2Cu_3O_7$

A. Kottmann, R. Siebinger, P. Lamparter, and S. Steeb

Max-Planck-Institut für Metallforschung, Institut für Werkstoffwissenschaft, D-70174 Stuttgart, Federal Republic of Germany

Z. Naturforsch. **50a**, 935–941 (1995); received July 25, 1995

The high temperature superconductor $YBa_2Cu_3O_7$ is characterized by a very anisotropic structure. The electronic structure of this compound is studied using high resolution valence band spectroscopy within an electron probe microanalyzer. From single crystals and melt-textured specimens, orientation dependent Cu–L_α spectra are obtained using a beryl crystal. The Cu–L_α spectra with polarization parallel to the z-direction show a larger energetic breadth compared to those obtained with polarization perpendicular to z. This is caused by occupied Cu $3d_{3z^2-r^2}$ like states, as could be shown by other workers using cluster calculations.

With a chlinochlore crystal, the polarized O–K_α spectra can be used to investigate the orientation of single crystal areas. The spectra map the bandlike O2p states. In contrast to the Cu–L_α spectra, the partial O–K_α spectra agree with band structure calculations in the local density approximation done by other workers.

Introduction

For the microscopic comprehension of material properties, knowledge of the electronic structure is essential. X-ray emission spectroscopy (XES) examines the occupied electronic states. With O–K_α and Cu–L_α spectra the O2p and Cu3d valence band state of copper-oxide superconductors can be probed separately.

Electron probe microanalysis (EPMA) [1, 2] focuses an electron beam on very small regions and, according to the large information depth of X-rays, probes the bulk properties.

The specimen spots from which the spectra are recorded, can be investigated directly concerning their oxygen content and stoichiometry.

By studying the orientation dependence of the emission bands from untwinned regions of single crystal or textured materials, additional information is obtained concerning the symmetry of Op2 or Cu3d states, which are determined by the magnetic quantum number m.

Thus, in the case of the O–K_α-emission line, the O_{px}-, O_{py}-, and O_{pz}-state can be measured. With the Cu–L_α-emission line the single d-orbitals contribute according to their weight to the intensity components I_x, I_y or I_z, which leads to a rather complicated correlation with the density of states.

Reprint requests to S. Steeb.

Presently the calculation of band structures has reached a high accuracy and it is possible to calculate partial densities of states. The comparison of such calculated results with the experimental data yields hints on how far the corresponding model describes the real facts and which states contribute to the different structural features of the observed spectra.

Theoretical Fundamentals

1. X-ray Emission and Density of States

In the electron microprobe the specimen is excited by electron impact, causing the formation of vacancies in core levels which are filled up by electronic transitions from the valence band following the electric dipole selection rules. This may lead to the emission of X-rays with the quantum energy $h\nu$. The total intensity of this radiation is given in the one electron- and dipole-approximation [3, 4] by

$$I(\nu, \boldsymbol{e}) \sim \nu^3 \sum_i \cdot \int_{Bz} | < \Psi_c(\boldsymbol{r}) | \boldsymbol{e} \cdot \boldsymbol{r} | \Psi_{ik}(\boldsymbol{r}) > |^2 \delta [E_i(\boldsymbol{k}) - E_c - h\nu] \, \mathrm{d}^3 \boldsymbol{k}, \quad (1)$$

where

$\boldsymbol{e}$ = unit vector of the polarization,
i = band index,
Bz = Brillouin zone,
Ψ_c = wave function of the core state,

0932-0784 / 95 / 1000-0935 $ 06.00 © – Verlag der Zeitschrift für Naturforschung, D-72027 Tübingen

Ψ_{ik} = wave function of the valence band state,
$\boldsymbol{r}$ = position vector in real space,
$\boldsymbol{k}$ = wave vector ($k = 2\pi/\lambda$),
$E_i(\boldsymbol{k})$ = energy of the valence band state,
E_c = energy of the core level state.

If the matrix element $|<\Psi_c|\boldsymbol{e}\cdot\boldsymbol{r}|\Psi_{ik}>| = |W_{ci}|$ is assumed to be independent of the wave vector [2], (1) can be written as

$$I(v, \boldsymbol{e}) \sim v^3 |W_{ci}|^2 \cdot D_i(E), \tag{2}$$

where

$|W_{ci}| = |<\Psi_c|\boldsymbol{e}\cdot\boldsymbol{r}|\Psi_{ik}>|$ = transition matrix element and $D_i(E)$ = electronic density of states. According to (2) the intensity yields the electronic density of states.

Since there is an electronic transition between two energetic states at one atomic site, X-ray emission is governed by strong electric dipole selection rules for these transitions. With $\Delta l = \pm 1$, the O–K_α emission valence band spectrum results from states with $l = 1$ symmetrie (O2p-states), the Cu–L_α spectrum results from states with $l = 2$ symmetrie (Cu 3d-states) or $l = 0$.

For the emitted radiation and its direction of polarization the magnetic quantum number m must be taken into account: $\Delta m = 0, \pm 1$. In the case of the orthorhombic structure of single crystalline $YBa_2Cu_3O_7$ the crystallographic axes of the specimen under investigation are chosen as a principal coordinate system [5]. Then the emitted intensity $I(v, \boldsymbol{e})$ can be decomposed into three components: $I_x = I(v, \boldsymbol{e} \parallel \boldsymbol{x})$, $I_y = I(v, \boldsymbol{e} \parallel \boldsymbol{y})$ and $I_z = I(v, \boldsymbol{e} \parallel \boldsymbol{z})$, with the polarization unit vector $\boldsymbol{e}$ of the electrical field aligned along the $\boldsymbol{x}$-, $\boldsymbol{y}$- and $\boldsymbol{z}$-direction, respectively. The X-ray intensity with a certain direction of polarization as emitted from a single crystal can be described by these partial intensities $I_x(v)$, $I_y(v)$, and $I_z(v)$ which depend, of course, on the specimen orientation relative to the direction of emission. Furthermore, they can be calculated starting from (1) with $\boldsymbol{e}\cdot\boldsymbol{r} = x$, y or z, respectively.

2. *Polarized O–K_α Emission and Band Structure Calculations*

According to [6] one obtains for the partial intensities in the case of K_α-X-ray emission

$$I_\eta(v) \sim v^3 R^2_{1s,p}(E) \cdot D_{p\eta}(E) \tag{3}$$

with $\eta = x, y, z$ and $R_{1s,p}(E)$ = matrix element, which depends on the radial contribution of the wave function. This radial component of the transition probability shows only a weak dependence on the energy E of the valency electrons [7] and yields no additional structures within the spectra.

Unpolarized spectra as obtained during the investigation of polycrystalline specimens yield the total density of states $D_{2p}(E)$, whereas the partial intensities $I_x(v)$, $I_y(v)$, and $I_z(v)$, respectively, reflect the partial densities of state $D_{px}(E)$, $D_{py}(E)$, and $D_{pz}(E)$. These densities correspond to the orbitals of the valence band with the quantum numbers $l = 1$ and $m = 1, -1$, and 0, respectively.

3. *Polarized Cu–L_α Emission and Band Structure Calculations*

Experimental and theoretical investigations of polarized X-ray emission are rare. The angle-dependent transition probabilities for tetragonal symmetry have been calculated in [8]. These calculations were applied in [9] for YBCO. For the contributions expressed in relative weighting factors of the single orbital group to the polarized L_α intensities $I_\eta(v)$ ($\eta = xy, z$) the following results were deduced:

i) The partial intensity $I_{xy}(\boldsymbol{e} \perp \boldsymbol{c})$ results mainly from electronic transitions from states with symmetry $3d_{x^2-y^2}$ (weighting factor 1) together with contributions from states with symmetry $3d_{xy}$, $3d_{xz}$, and $3d_{yz}$ (weighting factor 0.4) and states with symmetry $3d_{3z^2-r^2}$ (weighting factor 0.25).
ii) The partial intensity $I_z(\boldsymbol{e} \parallel \boldsymbol{c})$ results from electronic transitions from states with symmetry $3d_{3z^2-r^2}$ (weighting factor 1) together with contributions from states with symmetry $3d_{xz}$ and $3d_{yz}$, respectively (weighting factor 0.75).
iii) Possible transitions from 4s-like valency band states show no effect of orientation.

4. *The Cu–L_α Emission Spectrum as treated with Cluster and Impurity Models, respectively*

According to [10] the possible starting states for the Cu–L_α X-ray emission are the $2p_{3/2}$ XPS final states. In [11] the Cu 3d correlations are treated by the "Anderson impurity model" and the Cu–L X-ray emission is a coherent optical process of second order [12, 13]. Then, by consideration of the symmetry, the following two possible paths for the Cu–L-emission have to be considered:

$$|\mathrm{Cu}\mathbf{2p}\,3d^{10}\mathbf{L}> \rightarrow |\mathrm{Cu}3d^9\mathbf{L}>, \tag{4}$$

$$|\mathrm{Cu}\mathbf{2p}\,3d^9> \rightarrow |\mathrm{Cu}3d^8>. \tag{5}$$

Table 1. Cu L_α XES-spectra with 4 kV electron energy. Full Width at Half Maximum (FWHM) and position of the peak maximum [14].

Compound	FWHM [eV]	Peak position [eV]
$YBa_2Cu_3O_7$	3.2 eV	929.5 eV
CuO	2.2 eV	929.1 eV
Cu_2O	3.4 eV	929.2 eV
Cu-metal	3.9 eV	929.7 eV

According to [11] the transition (4) dominates and determines the peak position of Cu–L_α.

Table 1 shows the Full Width at Half Maximum (FWHM) and the peak position of the measured Cu–L_α X-ray emission lines as obtained for the corresponding compounds and Cu-metal, respectively.

Experimental

1. Spectrometer Crystals

The X-ray emission spectra were determined with an electron microprobe (JEOL JXA-733) where the O–K_α radiation is excited by an electron beam with 10 kV and 0.6 μA and the Cu–L_α radiation with 4 kV or 10 kV and 0.4 μA. For the determination of the O–K_α and Cu–L_α spectra the spectrometer crystals chlinochlore (CCL) and beryl (BER) were used [15, 16]. The spectrometer crystal acts as a wavelength dispersive element according to Bragg's law and furthermore as an analyzer for polarized radiation.

According to Brewster's law, for the Bragg angle $\Theta = 45°$ one observes for the reflected radiation a totally linearly polarized beam with the polarization direction vertical to the plane of incidence (= spectrometer plane – SP). The component of the incoming radiation which is polarized in the spectrometer plane is not reflected.

Both spectrometer crystals, CCL (orientation (001), $2d = 2.84$ nm) and BER (orientation $(00\bar{1}0)$, $2d = 1.59$ nm) map the O–K_α and Cu–L_α spectra in the angular range of $56° \leq \Theta \leq 57°$. The energy resolution amounts to about 0.5 eV. The intensity $I(\nu)$, as measured by the proportional counter, is the sum of the vertical and parallel polarized intensity components, and we obtain

$$I(\nu) \sim I^r(\nu, e \perp \mathrm{SP}) + I^r(\nu, e \parallel \mathrm{SP}) \sim I^0(\nu, e \perp) + pI^0(\nu, e \parallel), \quad (6)$$

where $I^r(\nu, e \parallel \mathrm{SP})$ is the reflected intensity of radiation with quantum energy $h\nu$ and direction of polarization parallel to the spectrometer plane, $I^r \sim I^r(\nu, e \perp \mathrm{SP})$ is the reflected intensity polarized perpendicular to the spectrometer plane, and I^0 the intensity emitted from the specimen. According to the classical electromagnetic theory for the special case of scattering of unpolarized X-rays from free electrons (Thomson formula [17]) we obtain for the so-called polarization ratio p:

$$p = (\cos 2\Theta)^2, \quad (7)$$

This relationship is valid for a perfect mosaic crystal, whereas for an ideal single crystal p amounts to $|\cos 2\Theta|$, [18, 19].

2. Apparatus

Figure 1 shows the spectrometer of the electron microprobe with the single crystal specimen S, spectrometer crystal C, and detector D arranged on the Rowland circle R with a radius of 140 mm. The spectrometer plane is identical with the plane of incidence of the spectrometer crystal and with the drawing plane in Figure 1. The determination of the partial intensity components $I_\eta(\nu)$ polarized parallel to the crystallographic axes of the single crystal sample, is performed by different well defined geometrical arrangements of the single crystal specimen relative to the spectrometer crystal and detector. Figure 1 shows one possible arrangement of the single crystal specimen S with the x-axis perpendicular to the spectrometer plane. The incident electron beam e^- is parallel to the z-axis, which is normal to the specimen surface.

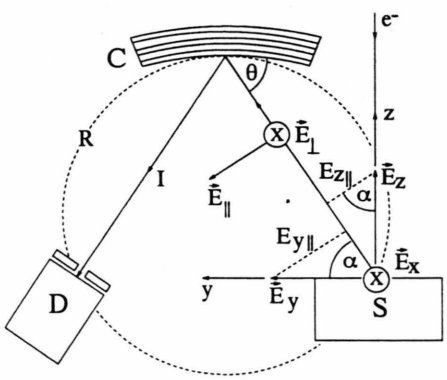

Fig. 1. Schematic presentation of the electron- and the X-ray beam path: single crystal specimen S, spectrometer crystal C, and detector D. The electric field components of the generated X-rays parallel to the x-, y-, z-axes as well as parallel (∥) or perpendicular (⊥) to the spectrometer plane are presented schematically.

The generated X-rays are observed at the take-off angle α. In the present case with an untilted specimen holder the take-off angle α amounts to 40°. With this geometrical arrangement the intensity components $I^0(\nu, e\perp)$ and $I^0(\nu, e\parallel)$ of the generated X-rays are expressed in terms of the partial intensities I_η. For the specific arrangement shown in Fig. 1 we obtain for the total measured intensity

$$I(\nu) = I^0(\nu, e\perp) + pI^0(\nu, e\parallel)$$
$$= I_x + p(I_y \sin^2\alpha + I_z \cos^2\alpha) \quad (8)$$

Since the x-axis is perpendicular to the spectrometer plane, the measured intensity $I(\nu)$ is dominated by the partial intensity I_x. With three different orientations of a single crystal specimen with orthorhombic structure one obtains the partial intensities I_x, I_y, and I_z.

3. *Specimens*

Extensive orientation-dependent Cu–L_α studies were done with single crystals and melt-textured $YBa_2Cu_3O_7$ samples [20, 21].

The textured samples are characterized by a typical diameter of about 2 cm, a large dimension of about 1 cm in the z-direction and single crystalline areas up to a diameter of 0.5 cm. The sintering process involving four steps is described in [22]. For the melting process the same temperature program as used for single crystal preparation [23] was applied under air atmosphere. With a temperature gradient during preparation, the z-axis of the melt-processed sample will be aligned to this temperature gradient [24]. In contrast to common polycrystalline samples, the grains show a well parallel aligned orientation of the c-axis, examined with X-ray diffraction, scanning electron microscopy, Laue images, and polarization microscopy.

Furthermore, the samples were treated in oxygen atmosphere in order to achieve an oxygen stoichiometry of nearly 7 and a T_C of 90 K (SQUID-measurements). Various annealing parameters were tested, the optimum was found for 100 h at 450 °C.

The composition of the specimens was investigated using electron microprobe analysis and X-ray diffraction. Figure 2 shows the X-ray diffraction patterns of melt textured $YBa_2Cu_3O_7$ after O_2-loading for 200 h (c) and 100 h (d) and the diffraction pattern of polycrystalline $YBa_2Cu_3O_7$ (e). The comparison with the three JCPDS-patterns from $BaCuO_2$ (a), Y_2BaCuO_5 (b), and $YBa_2Cu_3O_7$ (f), respectively, shows that there

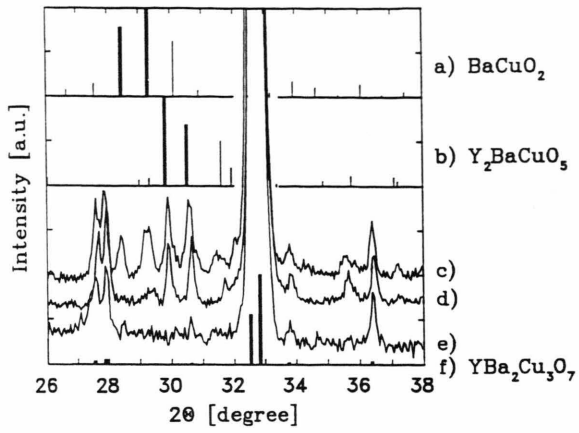

Fig. 2. X-ray diffraction (CuK_α): c) $YBa_2Cu_3O_7$ after 200 h O_2-loading, d) $YBa_2Cu_3O_7$ after 100 h O_2-loading, e) $YBa_2Cu_3O_7$ polycrystalline [22]. JCPDS-patterns for comparison: a) $BaCuO_2$, b) Y_2BaCuO_5, f) $YBa_2Cu_3O_7$

are inclusions of the green phase Y_2BaCuO_5 and of $BaCuO_2$. The share of the latter phase increases with annealing times over 100 h. Most of the Y_2BaCuO_5 inclusions have a round shape and dimensions up to 5 micrometer.

Results and Discussion

For a detailed presentation of the present results we refer to [25].

1. *Melt textured YBCO: $e\parallel c$ and $e\perp c$*

Figure 3 shows the run of the Cu–L_α spectra versus the X-ray quantum energy using a take off angle of 90° and 40°, respectively. Each plot consists of twenty measuring points, which were obtained from different specimen points but with the same specimen orientation. The energy of the primary electrons was 10 keV, which is sufficient to exclude surface effects and to maintain constant conditions of excitation.

The position of the maximum lies at 929.5 eV for all partial spectra and corresponds to the value of 929.7 eV for metallic Cu. For both take off angles the I_z spectrum is broader than the I_{xy} spectrum and shows a shoulder at 930.7 eV. We mention that all Cu–L_α spectra either from polycrystalline or single crystalline specimens are asymmetric. Going from $\alpha = 90°$ to $\alpha = 40°$, the Full Width at Half Maximum (FWHM) decreases for I_{xy} from 3.0 eV to 2.7 eV and

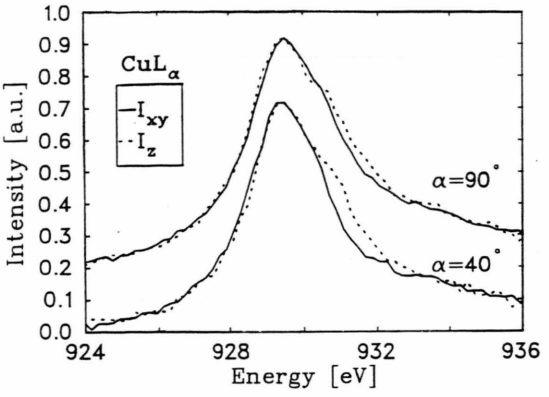

Fig. 3. Melt textured YBCO. Partial Cu–L_α spectra. Take off angle $\alpha = 90°$ (upper curves) and 40° (lower curves). —— $= I_{xy}$, – – – $= I_z$.

for I_z from 3.2 eV to 3.0 eV. This effect is caused by the self absorption [26].

From Fig. 3 follows that only those partial emission spectra should be compared which were obtained with the same experimental conditions for excitation and absorption [27]. For the high T_C superconductor $(La_x Sr_{1-x})_2CuO_4$ the influence of the Coulomb interchange energy on the Cu–L_α emission spectrum was treated in [11]. For a value of 8 eV for this energy the FWHM amounted as in the present case to 3.4 ± 0.2 eV, and the Cu–L_α spectrum showed a shoulder at higher energies. The interchange energy of 8 eV leads to an energy difference between the peak position of the Cu–L_α emission and absorption spectra, respectively, which amounts to about 1.5 eV [14] for YBCO and to about 1.8 eV [28] for La_2CuO_4. The relatively high value of 8 eV leads to the conclusion that copper of valency three does not occur in these alloys.

In [29] the influence of the charge transfer energy on the Cu–L_α shoulder is discussed. The authors show that a decrease of this energy causes a decrease of the shoulder. The value of 2.3 eV for the charge transfer energy leads to a shoulder form as observed in Figure 3.

Cu–L_α spectra for CuO and La_2CuO_4 were calculated in [29] according to the "Anderson impurity" model. CuO yields a narrow nearly symmetrical Cu–L_α spectrum, as also observed in [30]. The calculations for the superconductor La_2CuO_4, however, lead to the formation of a shoulder as also observed for YBCO (see Fig. 3, for example).

2. Untwinned regions of YBCO single crystals: $e \parallel a$ and $e \parallel b$

With untwinned ab faces of YBCO single crystals, O–K_α spectra as well as Cu–L_α spectra were obtained and presented in Figs. 4a and 4b. The partial I_x spectra were observed with $e \parallel a$, for I_y stands $e \parallel b$, and the spectra are plotted versus the binding energy using for the position of the inner O1s-niveau the value 528.5 eV from XPS data [32]. The run of the I_x- and I_y-spectra in Fig. 4a can be understood according to calculations [33] of the density of states according to the OLCAO-method (Orthogonalized Linear Combination of Atomic Orbitals). According to this, the run of the density of states is mainly caused by the strong Cu3d–O2p σ-bonds within the CuO_2-planes, whereas the Cu–O chains along the y direction yield the pronounced shoulder at 4.5 eV in the run of I_y (Figure 4a). For a further discussion and presentation also of the O–K_α I_z-spectrum see [16, 30].

Figure 4b shows the $I_x(e \parallel a)$, $I_y(e \parallel b)$, and $I_z(e \parallel c)$ partial Cu–L_α emission spectra versus the binding energy. From XPS data [31] follows for the position of

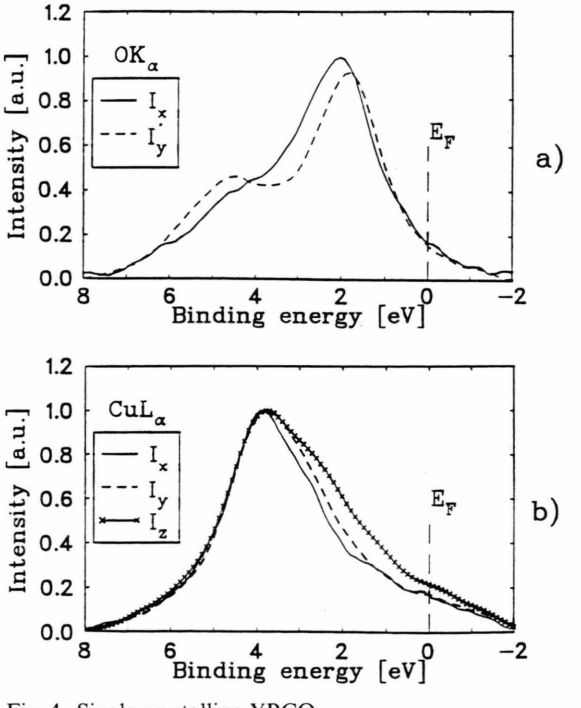

Fig. 4. Single crystalline YBCO.
a) Partial O–K_α spectra: —— $= I_x(e \parallel a)$, – – – $= I_y(e \parallel b)$;
b) Partial Cu–L_α spectra: —— $= I_x(e \parallel a)$, – – – $= I_y(e \parallel b)$, x–x–x $= I_z(e \parallel c)$.

the inner $Cu2p_{3/2}$ niveau 933.3 eV. Each plot consists of 20 to 30 single measurements. The position of the maxima of the Cu3d and O2p states on the binding energy scala is in agreement with the valence band XPS spectra [32].

I_z shows the largest FWHM of 3.4 eV and a pronounced shoulder at 2 eV. The FWHM for I_y and I_x is 2.8 eV and 2.6 eV, respectively. The position of the main maximum at 3.8 eV and the run at higher binding energies is the same for the three partial spectra in Figure 4b.

The comparison of the experimental runs of the partial $Cu-L_\alpha$ spectra with the Cu3d density of states as calculated by band structure calculations [33] shows distinct differences in the maximum position and also in the run at higher binding energies.

The comparison of the experimental data with those obtained from the calculations according to the Local Density Approximation (LDA) [34] does not show good accordance.

The experimental partial spectra show a rather smooth run. This means that apparently relaxation processes and transition probabilities dominate. Thus the calculations never may represent ground state valency band states during the $Cu-L_\alpha$ emission. Furthermore, the defect electron as produced during the excitation within the inner Cu2p niveau must be regarded. Probably this hole causes just before the X-ray emission process relaxation- and shielding processes. Thus it will be necessary for the explanation of the I_x-, I_y-, and I_z-spectra of Fig. 4b, to apply the "Anderson impurity" model, for example, with view to the excited state just before the X-ray emission.

Summary

The $O-K_\alpha$- and $Cu-L_\alpha$ X-ray emission spectra of the high temperature superconductor $YBa_2Cu_3O_7$ are dominated by the complex electronic structure of this compound. The band-like O2p states are well described. The comparison with the result of LDA-calculations works well. The observed $Cu-L_\alpha$ spectra show the strong localized character of the Cu3d states with their high Coulomb interchange energy of about 8 eV. The comparison with LDA-band structure calculations shows no good correlation. Improved calculations should take into account the defect electron within the inner Cu2p level which is produced during the excitation of the corresponding atom. This could be done in the frame of cluster calculations and using the "Anderson impurity" model. The latter describes the measured partial $Cu-L_\alpha$ spectra with $\boldsymbol{e} \parallel \boldsymbol{c}$ and $\boldsymbol{e} \perp \boldsymbol{c}$ correct, but not the $Cu-L_\alpha$ spectra with $\boldsymbol{e} \parallel \boldsymbol{a}$ and $\boldsymbol{e} \parallel \boldsymbol{b}$.

[1] F. Burgäzy, H. Jaeger, K. Schulze, P. Lamparter, and S. Steeb, Z. Naturforsch. **44a,** 180 (1989).
[2] G. Dräger and O. Brümmer, Phys. Status Solidi B **124,** 11 (1984).
[3] B. K. Agarwal, X-Ray Spectroscopy. Springer-Verlag, Berlin 1979.
[4] L. V. Azároff, X-Ray Spectroscopy. McGraw-Hill, London, 1974.
[5] P. Rennert, Th. Dörre, and U. Gläser, Phys. Stat. Sol. (B) **87,** 221, (1978).
[6] G. Dräger, F. Werfel, and J. A. Leiro, Phys. Rev. B **41,** 4050 (1990).
[7] D. A. Goodings and R. Harris, J. Phys. C **2,** 1808 (1969).
[8] A. Šimůnek and G. Wiech, Phys. Rev. D **30,** 923 (1984).
[9] H.-O. Feldhütter, A. Šimůnek, and G. Wiech, Solid State Comm **79,** 977 (1991).
[10] M. Fujinami, H. Hamada, Y. Hashiguchi, and T. Ohtsubo, Japan J. Appl. Phys. **28,** 1959 (1989).
[11] S. Tanaka, K. Okada, and A. Kotani, J. Phys. Soc. Japan **58,** 813 (1989).
[12] P. W. Anderson, Phys. Rev. **124,** 41 (1961).
[13] A. Kotani and K. Okada, Progress of Theoretical Physics, Supplement **101,** 329 (1990).
[14] A. Kottmann, Doctor Thesis, University of Stuttgart, 1994.
[15] F. Burgäzy, Doctor Thesis, University of Stuttgart, 1990.
[16] A. Kottmann, F. Burgäzy, D. J. Lam, Y. Fang, P. Lamparter, and S. Steeb, Physica C **178,** 125 (1991).
[17] A. Guinier, X-Ray Diffraction. W. H. Freeman & Company, London 1963.
[18] D. Stephan and W. Löschau, Kristall und Technik **11,** 1295 (1976).
[19] N. M. Olekhnovich, Kristallografija **18,** 1240 (1973).
[20] M. Murakami, Supercond. Sci. Technol. **5,** 121 (1992), and references therein.
[21] Thanks are due to H. Kronmüller from this Institute for supplying us with these samples.
[22] Th. Schuster, M. R. Koblischka, B. Ludescher, R. Henes, A. Kottmann, and H. Kronmüller, Materials Letters **14,** 189 (1992).
[23] C. Thomsen, M. Cardona, B. Gegenheimer, R. Liu, and A. Simon, Phys. Rev. B **37,** 9860 (1988); M. R. Koblischka, Doctor Thesis, University of Stuttgart, 1992.
[24] M. Ullrich, D. Müller, K. Heinemann, L. Niel, and H. C. Freyhardt, Physica C **198,** 181 (1992).
[25] R. Siebinger, Diploma Thesis, University of Stuttgart, 1994.
[26] S. Hanzely and R. J. Liefeld; in Bernett (ed.), Electronic Density of States (1971), NBS Spec. Publ. No. 323.
[27] F. Werfel, G. Dräger, J. A. Leiro, and K. Fischer, Phys. Rev. B **45,** 4957 (1992).
[28] F. Burgäzy. Unpublished experiments.

[29] S. Tanaka, K. Okada, and A. Kotani, J. Phys. Soc. Japan **60,** 3893 (1991).
[30] A. Kottmann, P. Lamparter, and S. Steeb, Mikrochim. Acta **114/115,** 343 (1994).
[31] P. Steiner, V. Kinsinger, L. Sander, B. Siegwart, S. Hüfner, C. Politis, R. Hoppe, and H. P. Müller, Z. Physik B **67,** 497 (1987).
[32] A. J. Arko, R. S. List, R. J. Bartlett, S.-W. Cheong, Z. Fisk, J. D. Thompson, C. G. Olson, A.-B. Yang, R. Liu, C. Gu, B. W. Veal, J. Z. Liu, A. P. Paulikas, K. Vandervoort, H. Claus, J. C. Campuzano, J. E. Schirber, and N. D. Shinn, Phys. Rev. B **40,** 2268 (1989).
[33] W. Y. Ching, J. Amer. Ceram. Soc. **73,** 3135 (1990).
[34] J. Redinger, A. J. Freeman, J. Yu, and S. Massidda, Phys. Lett. A **124,** 469 (1987).